



Spectroscopic characterization of a new Re(I) tricarbonyl complex with a thiosemicarbazone derivative: towards sensing and electrocatalytic applications

Journal:	<i>Dalton Transactions</i>
Manuscript ID	DT-ART-03-2020-001078.R1
Article Type:	Paper
Date Submitted by the Author:	28-Apr-2020
Complete List of Authors:	Souza, Breno; Universidade Federal de Uberlandia Instituto de Quimica Faustino, Leandro; Universidade Federal de Uberlandia Instituto de Quimica Prado, Fernando; Universidade Federal de Uberlandia Instituto de Quimica Sampaio, Renato; Brookhaven National Laboratory, Chemistry Division da Silva Maia, Pedro; Universidade Federal do Triangulo Mineiro, Chemistry Hora Machado, Antonio Eduardo; Universidade Federal de Uberlandia, Instituto de Química PATROCINIO, ANTONIO OTAVIO; Universidade Federal de Uberlandia Instituto de Quimica,

**Spectroscopic characterization of a new Re(I) tricarbonyl complex
with a thiosemicarbazone derivative: towards sensing and
electrocatalytic applications†**

Breno L. Souza¹, Leandro A. Faustino¹, Fernando S. Prado¹, Renato N. Sampaio², Pedro I. S. Maia³, Antonio Eduardo H. Machado¹, Antonio Otavio T. Patrocínio^{1*}

¹ Laboratory of Photochemistry and Materials Science, Institute of Chemistry, Universidade Federal de Uberlândia, 38400-902, Uberlândia, Brazil

² Chemistry Division, Energy & Photon Sciences Directorate, Brookhaven National Laboratory, Upton, USA

³ Núcleo de Desenvolvimento de Compostos Bioativos (NDCBio), Universidade Federal do Triângulo Mineiro, Av. Dr. Randolpho Borges 1400, 38025-440 Uberaba, MG, Brazil

*To whom the correspondence should be addressed:

otaviopatrocinio@ufu.br

†Electronic supplementary information (ESI) available. See DOI: XXX

Abstract

This work describes the preparation of a new thiosemicarbazone derivative, (Z)-N-ethyl-2-(6-oxo-1,10-phenanthroline-5(6H)-ylidene)hydrazinecarbothioamide (phet) and its respective Re(I) tricarbonyl chloro complex, *fac*-[ReCl(CO)₃(phet)]. The spectroscopic, photophysical and electrochemical properties of the new complex were fully investigated through steady state and time-resolved techniques along with computational calculations. In *fac*-[ReCl(CO)₃(phet)], the new ligand is coordinated to the metal center through the pyridyl rings of the phenanthroline moiety. The unbound electron pairs in the S atom of the bending thiosemicarbazone group induce new low energy lying electronic transitions. Consequently, enhanced visible light absorption up to 550 nm is observed in acetonitrile due to the overlap between MLCT_{Re→phet} and I_{phet(n→π*)} transitions. The absorption bands and emission quantum yields of *fac*-[ReCl(CO)₃(phet)] are sensitive to proton concentration due to an acid-basic equilibrium in the N atoms of the thiosemicarbazone. Proton dissociation constants of 10.0 ± 0.1 and 11.4 ± 0.2 were determined respectively for the ground and excited states of the new complex. Spectral changes could also be observed in the presence of Zn²⁺ cations which can be further explored for sensing applications. The electrochemical behavior of the new complex was studied in detail, revealing up to four one electron reduction processes in the range from 0 to -2.4 V vs Fc⁺/Fc. With support of DFT calculations, the first three processes are ascribed to the reduction of the coordinated phet ligand followed by the Re^{I/0} reduction and consequent Cl⁻ release. The new complex was able to act as electrocatalyst for CO₂ reduction into CO ($E_{\text{onset}} = -1.92$ V vs Fc⁺/Fc), with a turnover frequency of 2.81 s⁻¹ and turnover number of 24 ± 1 in anhydrous acetonitrile, being the first Re(I) tricarbonyl complex with a thiosemicarbazone derivative described for this goal. The detailed characterization carried out here can drive the development of new Re(I)-thiosemicarbazone derivatives for different applications.

Keywords: CO₂ reduction, Re(I) complexes, electrocatalysis, photophysics

1. Introduction

The interest in Re(I) coordination compounds of general formula *fac*-[ReL(CO)₃(NN)], NN = diimine ligands, L = ancillary ligand, has increased since the early works by Whrighton and Morse in the 1970s¹⁻⁴. These complexes exhibit interesting photochemical and photophysical properties, which can be largely modulated by ligand selection. As a result, different applications have emerged, such as sensing⁵⁻⁷, light-emitting devices⁸⁻¹¹, photoswitches¹²⁻¹⁴ catalysis¹⁵ and as biomarkers^{16,17}.

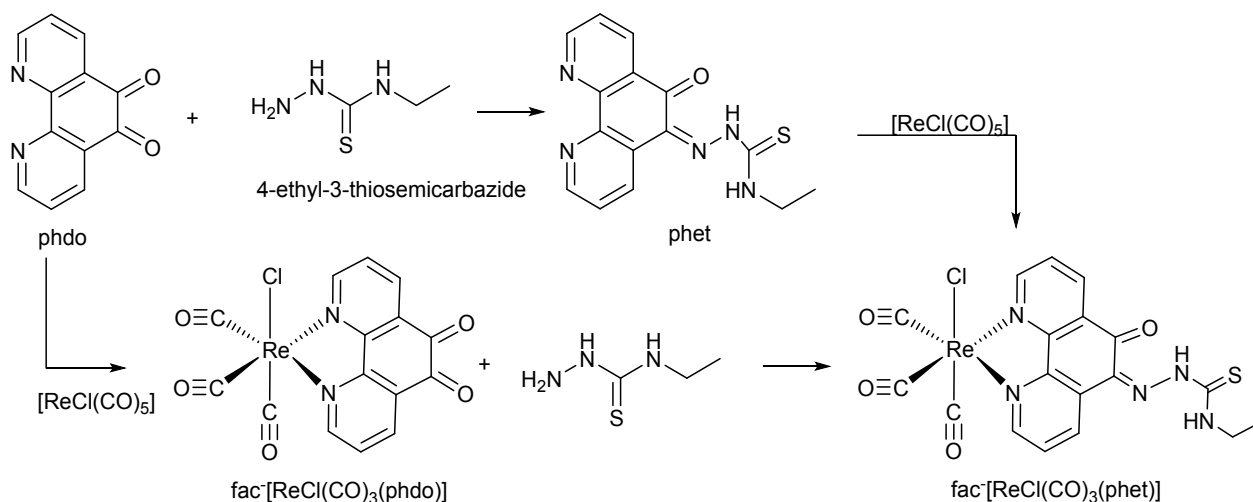
Particularly, Re(I) complexes have been recognized by their ability to reduce CO₂, both photo- and electrochemically¹⁸. Their catalytic activity was first described by Sacksteder and Lehn¹⁹ employing the *fac*-[ReCl(CO)₃(bpy)] complex, bpy = 2,2'-bipyridine and, since then, several research groups have investigated the mechanistic aspects of this reaction aiming at development of more efficient Re(I)-based CO₂ reduction catalysts^{12,20-25}. Lehn's system could efficiently and selectively catalyze the electrochemical conversion of CO₂ to CO. More recently, Ishitani's group reported the preferential formation of formate in aqueous CO₂ solutions also employing a Re(I) polypyridyl complex as catalyst²⁶. By the selection of the ligands surrounding the metal center, one can not only control the product selectivity as well as improve the kinetics of the gas conversion. Typically, the addition of electron donor groups to the polypyridine ligand yields a higher nucleophilicity in the Re(I) center, leading to a better activity towards CO₂ reduction^{27,28}.

Re(I) tricarbonyl complexes employing hydrazonic ligands are still poorly explored in the literature. These ligands are characterized by a [C=N-NH-C=X] moiety, where X = S, Se or O and can also contain pyridyl rings, offering multiple coordination sites. These ligands have been explored as cytotoxic agents and their biological activity is strongly affected by metal coordination²⁹. Abram and Lopez, for example, reported air stable N,N,S-bounded thiosemicarbazone Re(I) complexes³⁰⁻³² which were later applied as estrogen receptors³³.

In a different approach, Bakir et al have reported Re(I) complexes with di-2-pyridylketone semicarbazone³⁴ and di-2-pyridylketone thiosemicarbazone

³⁵, in which the metal center is coordinated by the pyridyl rings in a *N, N* configuration. The complexes exhibit intense visible light absorption and the (thio)semicarbazone moiety offers sensitivity to the surrounding media with noticeable spectral changes in different solvents, proton concentrations and presence of other metallic cations. Both complexes also exhibit rich electrochemical behavior, although consecutive reductions lead to the irreversible loss of the hydrazone moiety.

In this work, a new ligand (*Z*)-*N*-ethyl-2-(6-oxo-1,10-phenanthroline-5(6*H*)-ylidene)hydrazinecarbothioamide (phet) based on the derivatization of 1,10-phenanthroline-5,6-dione (phdo) by 4-ethyl-3-thiosemicarbazide was engineered, Scheme 1. As it will be shown in this manuscript, the ligand was designed to combine the sensitivity of the low energy absorption transitions on the surrounding medium with multiple (quasi)reversible reduction processes. While the first property can be conveniently explored on the development of optical molecular probes, the later can introduce beneficial effects in accelerating multi-electron transfer processes on photo(electro)catalytic systems. Herein, the new ligand was reacted with $[\text{ReCl}(\text{CO})_5]$ to yield the novel tricarbonyl *fac*- $[\text{ReCl}(\text{CO})_3(\text{phet})]$ complex. The complex was fully characterized towards their spectroscopic, photophysical and electrochemical properties using steady-state and time-resolved techniques and further explored as CO_2 reduction electrocatalyst into CO, being the first Re(I) complex with a thiosemicarbazone derivative applied to this important reaction. The insights reported here can be further applied in the development of new derivatives for different applications in biology, sensing and catalysis.



Scheme 1. Synthetic approaches for the preparation of *fac*-[ReCl(CO)₃(phet)]

2. Experimental procedures

All employed solvents were HPCL grade. 4-ethyl-3-thiosemicarbazide, [ReCl(CO)₅] and tetrabutylammonium hexafluorophosphate were acquired from Aldrich and were used without purification. 1,10-phenanthroline-5,6-dione (phdo) was synthesized as previously described^{36–38}.

2.1. Syntheses

The new ligand, (Z)-N-ethyl-2-(6-oxo-1,10-phenanthroline-5(6H)-ylidene)hydrazinecarbothioamide (phet), was prepared by refluxing a mixture of 0.40 g (1.90 mmol) of phdo and 0.27 g (2.28 mmol) of 4-ethyl-3-thiosemicarbazide in 25 mL of ethanol (Aldrich), and 1 mL of concentrated HCl (12 mol L⁻¹). The crude product was collected by filtration and recrystallized from hot ethanol. Yield 95%. Anal. Calc. for C₁₅H₁₃N₅OS.H₂O: C, 54.70; H, 4.59; N, 21.26; S, 9.74. Found: C, 54.40; H, 4.37; N, 20.90; S, 9.34. ¹H NMR ((CD₃)₂SO, 400 MHz, d/ppm): 14.39 (s, 1H), 9.96 (t, 1H), 9.32 (dd, 1H), 9.23 (dd, 1H), 8.90 (dd, 1H), 8.69 (dd, 1H), 7.86 (m, 1H), 7.84 (m, 1H), 3.72 (m, 2H), 1.24 (t, 3H). FT-IR (ATR, cm⁻¹): ν(C=O) 1622; ν(C=S) 1168-1078, 846-800, 775-735; ν(N-H) 3400-3330; ν(N-N) 1045.

As shown in Scheme 1, the new complex *fac*-[ReCl(CO)₃(phet)] can be obtained by the reaction of phet with the precursor [ReCl(CO)₅] or, alternatively, from the condensation reaction between the 4-ethyl-3-thiosemicarbazide and the already coordinated phdo. This later route exhibited higher yields. In a

typical procedure, *fac*-[ReCl(CO)₃(phdo)] (0.42g; 0.81 mmol), synthesized as reported before ³⁹ and an excess of 4-ethyl-3-thiosemicarbazide (0.12 g; 0.98 mmol) were refluxed by 6h in 30 mL of ethanol (Aldrich) and 1 mL of concentrated HCl (12 mol L⁻¹). The as obtained red solid was filtered and purified by recrystallization from DMSO by dropwise addition of water. Yield 80%. Anal. Calc. for C₁₈H₁₃ClN₅O₄ReS: C, 35.04; H, 2.12; N, 11.35; S, 5.20. Found: C, 35.23; H, 2.15; N, 11.00; S, 4.95. ¹H NMR ((CD₃)₂SO, 400 MHz, d/ppm): 14,36 (s, 1H), 10,01 (t, 1H), 9,39 (dd, 1H), 9,35 (dd, 1H), 9,13 (dd, 1H), 8,92 (dd, 1H), 8,00 (m, 1H), 7,95 (m, 1H), 3,74 (m, 2H), 1,26 (t, 3H). HRMS-ESI analysis: theoretical [M-H]⁻ 615.9862; found: 615.9826. FT-IR (ATR, cm⁻¹): ν(C≡O) 2026, 1921 and 1885; ν(C=O) 1622; ν(C=S) 1160-1078, 785-750; ν(N-H) 3350-3300; ν(N-N) 1045; ν(Re-Cl) 267.

2.2. Spectroscopic and electrochemical measurements

Electronic absorption spectra were recorded in a Shimadzu UV-Visible spectrophotometer UV-1650 PC. ¹H NMR spectra were recorded in a Bruker Ascend 400 Mhz spectrometer. The residual peak from the solvent, (CD₃)₂SO, was used as internal standard. Electrospray ionization mass spectrometry was carried out in a Agilent 6520 B QTOF spectrometer. Samples were dissolved in 4:1 methanol/water mixtures and submitted to nebulization at 20 psi at 200 °C at a capillary flow of 8 L min⁻¹ under 4.5 kV. Attenuated total reflectance Fourier transformed infrared (ATR-FTIR) spectra were recorded in a Perkin Elmer Frontier spectrometer equipped with a diamond crystal plate, using 16 scans at a resolution of 4 cm⁻¹. Emission spectra were obtained in a Horiba Fluoromax-4 fluorimeter at room temperature. Solutions were purged with argon or oxygen during five minutes before the measurements. Quantum yield determination was carried out as described before ^{40,41} employing [Ru(bpy)₃]Cl₂ as standard (φ_{em} = 0.062) ⁴².

TRIR measurements were performed at Chemistry Department of the Brookhaven National Laboratory employing a setup described elsewhere ⁴³, Briefly CW external-cavity quantum cascade laser (EC-QCL model 21049-MHF) was used as probe light source in the 2150–2005 cm⁻¹ region. A Nd:YAG pulsed laser (SpectraPhysics, Quanta-Ray LAB-170-10, 8-10 ns FWHM)

coupled to an OPO (SpectraPhysics VersaScan) was used as the excitation light source at 450 nm. IR beam was split into reference and probe beams, with the latter passing through the IR cell. These beams were directed onto a matched pair of fast rise time IR detectors (Kolmar Technologies, Inc., KMPV9-0.5- J2, DC-20 MHz). The analog signals were simultaneously digitized on an oscilloscope (Teledyne LeCroy HDO 4034, 12-bit, 350 MHz, 2.5 GS/s) and normalized to remove noise from laser intensity fluctuations.

Spectroscopic titrations based on UV-visible absorption and photoluminescence measurements were performed to determine the ground and excited state acid-basic behaviors of the complex in acetonitrile at room temperature. In a 1 mmol L⁻¹ complex solution, aliquots of NaOH aqueous solutions (5 mmol L⁻¹) were added and the apparent pH (pH_{app}) variation monitored. The absorption and emission data were fitted to the equations 1 and 2⁴⁴⁻⁴⁶ respectively, in which pβ and pβ* are the proton dissociation constant of the ground and excited states respectively; A_{max} is the maximum absorbance at the selected wavelength; A_{min} is the minimum absorbance and A_i is the observed absorbance at a certain proton concentration; Φ_{max} is the maximum quantum emission yield for the deprotonated form; Φ_{min} is the minimum quantum emission yield for the protonated and Φ_i is the emission quantum yield at a certain proton concentration.

$$\text{pH}_{app} = \text{p}\beta + \log \frac{(A_i - A_{\min})}{(A_{\max} - A_i)} \quad (1)$$

$$\text{pH}_{app} = \text{p}\beta^* + \log \frac{(\Phi_i - \Phi_{\min})}{(\Phi_{\max} - \Phi_i)} \quad (2)$$

Electrochemical measurements were obtained in a μAutolab PGSTAT204 potentiostat/galvanostat (Autolab) using a glassy carbon as working electrode, a platinum wire as counter electrode, and Ag/AgCl 3 mol L⁻¹ KCl as the reference electrode. All measurements were carried out in Ar or CO₂ deaerated anhydrous acetonitrile or propylene carbonate with tetrabutylammonium hexafluorophosphate (0.1 mol L⁻¹) as supporting electrolyte. All potentials are presented *versus* Fc⁺/Fc (E⁰ = 0.400 V vs SHE). Controlled potential electrolyses at 298 K were carried out in a homemade gas tight H-cell (Figure S1). A graphite rod (6 mm diameter) was employed as

working electrode, Ag/AgCl 3 mol L⁻¹ KCl as reference electrode and a Pt grid as counter electrode. The applied potential was fixed to be 300 mV more negative than the onset potential. At a given electrolysis time, an aliquot of the overhead volume over the catholyte was taken and analyzed by gas chromatography (PerkinElmer Clarus 580, equipped with a porapak N 2mm and a TCD detector).

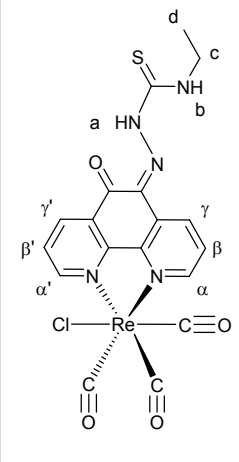
Theoretical calculations based on the Density Functional Theory (DFT) were performed employing the GH-mGGA Minnesota 2006 (M06) functional to geometry optimization in the Gaussian09 software. Oscillator strength for the main electronic transitions were obtained by the time-dependent Density Functional Theory (TD-DFT). Re(I) center was described with the relativistic SARC-DKH basis set, while the remaining atoms were described by the Def2-TZVPP basis set. All calculations were performed using an IEFPCM continuum solvation model and considering a solvent with inherent properties of CH₃CN⁴⁷.

3. Results and discussion

3.1. Spectroscopic Characterization

The new complex *fac*-[ReCl(CO)₃(phet)] can be obtained in satisfactory yield by two different routes. By refluxing the [ReCl(CO)₅] precursor with the previously synthesized phet ligand or by promoting the reaction between the thiosemicarbazide and *fac*-[ReCl(CO)₃(phdo)] in ethanol. The condensation reaction is catalyzed by addition of HCl and no secondary products are formed. Due to steric/kinetic effects, the insertion of two thiosemicarbazide into phdo seems to be hindered, even when a large excess of thiosemicarbazide is used. The structure and purity of the ligand and the new complex were confirmed by elemental analysis, FT-IR (Figure S2, Supporting information), ¹H NMR spectroscopy (Figure S3) and HRMS. In Table 1, a tentative attribution of the observed ¹H NMR peaks is presented. These attributions are corroborated by H-H COSY spectra (Figure S4 of Supporting Information), as well as HMBC and HSQC spectra of the free ligand, Figures S5 and S6.

Table 1. ^1H NMR spectral data for phet and *fac*-[ReCl(CO)₃(phet)]. (DMSO-*d*₆; 400 MHz)

	free PHET		<i>fac</i> -[ReCl(CO) ₃ (phet)]	
	Proton	δ / ppm	J / Hz	δ / ppm
H _{α}	8.90 (dd, 1H)	1.6; 4.8	9.13 (dd, 1H)	1.2; 4.8
H _{β}	7.84 (m, 1H)	-	7.95 (m, 1H)	-
H _{γ}	9.27 (d, 1H)	7.6	9.40 (d, 1H)	1.2; 8.1
H _{α'}	9.14 (dd, 1H)	1.7; 4.7	9.35 (dd, 1H)	1.2; 4.8
H _{β'}	7.86 (m, 1H)	-	8.00 (m, 1H)	-
H _{γ'}	8.69 (dd, 1H)	1.8; 8.0	8.93 (dd, 1H)	1.2; 7.8
H _a	14.39 (s, 1H)	-	14.36 (s, 1H)	----
H _b	9.96 (t, 1H)	6.0	10.01 (t, 1H)	6.0
H _c	3.72 (q, 2H)	7.0	3.74 (q, 2H)	7.0
H _d	1.24 (t, 3H)	7.2	1.26 (t, 3H)	7.2

In the phet, H _{γ} is deshielded in relation to H _{α} and H _{β} , which can be attributed to the influence of the thiosemicarbazone moiety. The same trend is observed in *fac*-[ReCl(CO)₃(phet)], in which the signals attributed to the protons of the pyridyl rings are deshielded in respect to the free phet ligand as the result of the coordination to the Re(I) center. The aliphatic hydrogens in phet are not largely affected by coordination as well as those bound to the nitrogen atoms in the hydrazonic moiety. For the free and coordinated ligand, H_a has a deshielded nucleus ($\delta > 14$ ppm). The observed chemical shift is higher than that observed for substituted thiosemicarbazones ($\delta = 8\text{--}11$ ppm^{48,49}) and it is attributed to the chemical environment in phet, with possible intramolecular interactions with the neighbor oxygen atom. In the same way, H_b is strongly influenced by the thione group and exhibits large chemical shifts in relation to the aromatic hydrogens.

The electronic absorption spectra of the free ligands phdo, phet and 4-ethyl-3-thiosemicarbazide and of *fac*-[ReCl(CO)₃(NN)], NN = phdo and phet, in CH₃CN are shown in Figure 1. The main peaks are listed at Table 2 along with those for the parental complex *fac*-[ReCl(CO)₃(phen)], phen = 1,10-phenanthroline⁵⁰.

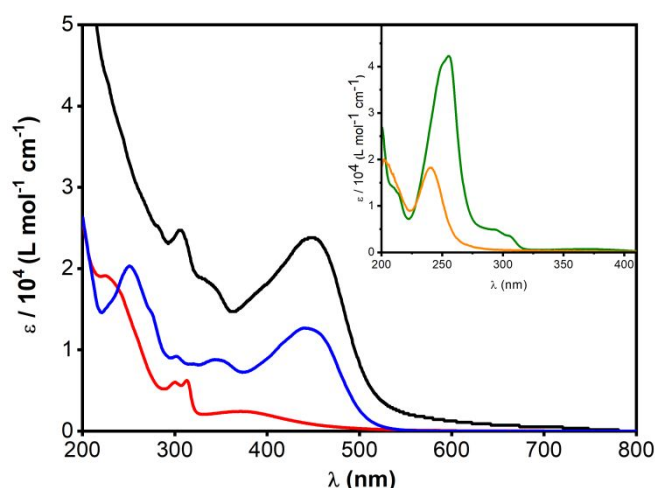


Figure 1. Electronic absorption spectra of the new complex *fac*-[ReCl(CO)₃(phet)] (—), the free ligand phet (—) and the complex *fac*-[ReCl(CO)₃(phdo)] (—) in CH₃CN. *Inset:* electronic absorption spectra of 4-ethyl-3-thiosemicarbazide (—) and the free phdo (—).

Table 2. Spectral parameters of the Rhenium(I) complexes and for the free ligands in CH₃CN.

Compound	λ_{\max} (nm) ($\epsilon / 10^4$ (L mol ⁻¹ cm ⁻¹))
4-ethyl-3-thiosemicarbazide	240 (1.82)
phen	230 (3.9), 263 (2.3)
<i>fac</i> -[ReCl(CO) ₃ (phen)] ¹	216 (4.4), 265 (2.6), 365 (0.34)
phdo	255 (4.20), 294 (0.50), 305 (0.35), 370 (0.07)
<i>fac</i> -[ReCl(CO) ₃ (phdo)]	225 (1.90), 301 (0.60), 313 (0.62), 372 (0.24)
phet	251 (2.03), 301 (0.92), 343 (0.88), 443 (1.27)
<i>fac</i> -[ReCl(CO) ₃ (phet)]	306 (2.47), 339 (1.82), 446 (2.38), 546 (0.24)

The novel phet ligand exhibits new absorption bands in the visible region of the spectrum that were not observed in phdo and the 4-ethyl-3-thiosemicarbazide themselves (Figure 2, inset). These low energy bands are associated with charge transitions between the thiosemicarbazone moiety and the phenanthroline rings. This assignment was confirmed by TD-DFT calculations, Table 3. Isosurface plots of selected molecular orbitals are available at Figure S7 of the supporting information. As expected, in the new ligand the electronic delocalization in the π orbitals are extended due the

introduction of the thiosemicarbazone group and, additionally the unbound electrons in the sulfur heteroatom strongly contribute to the stabilization of the frontier orbitals. As a result, the phet ligand exhibits absorption up to 500 nm.

After the coordination to the Re(I) center to form the *fac*-[ReCl(CO)₃(phet)] complex, an absorption tail ranging from 550 to 750 nm is observed and the molar absorptivity of the low energy band centered at 443 nm is enhanced. At higher energies the highly allowed absorption bands are assigned to polypyridyl intraligand transitions, $IL_{\text{phet}} (\pi \rightarrow \pi^*)$ ^{1,12,51}. As no shifts are observed in the low energy band in relation to the free phet ligand, one can expect a high contribution of $IL_{\text{phet}} (n \rightarrow \pi^*)$ to the visible light absorption in *fac*-[ReCl(CO)₃(phet)]. Moreover, the increase in the molar absorptivity in this region indicates the overlap between MLCT and $IL_{\text{phet}} (n \rightarrow \pi^*)$ transitions. This overlap is clearly seen when the spectral data for *fac*-[ReCl(CO)₃(phet)] are compared with those for *fac*-[ReCl(CO)₃(phen)] or *fac*-[ReCl(CO)₃(phdo)], Figure 1, Table 2. These complexes are well characterized in the literature^{1,39,50} and exhibit low energy symmetry forbidden MLCT transitions with molar absorptivities in the order of $10^3 \text{ L mol}^{-1} \text{ cm}^{-1}$. On the other hand, the molar absorptivity of the low energy bands in *fac*-[ReCl(CO)₃(phet)] are in the order of $10^4 \text{ L mol}^{-1} \text{ cm}^{-1}$, which is attributed to the overlap between $IL_{\text{phet}} (n \rightarrow \pi^*)$ and MLCT transitions.

TD-DFT calculations confirm the as-described assignments. The calculated main transitions for the new complex are listed at Table 3 and an energy diagram is presented at Figure 2 along with the respective molecular orbitals. A comparison between the theoretical and experimental electronic spectra is shown in Figure S8 of the Supporting Information.

Table 3. Selected energy electronic transitions for phet and *fac*-[ReCl(CO)₃(phet)] with their respective oscillator strengths (*f*) and associated energies.

Compound	State	Molecular orbitals (weights/%) ^a	<i>f</i>	Energy /eV (nm)	Character
phet	S ₁	H → L	0.0001	2.602 (476)	IL _n →π*
	S ₂	H-1 → L (46) H-3 → L (33)	0.1637	2.942 (421)	IL _n →π*/ IL _π →π*
	S ₃	H-1 → L (51) H-5 → L (33)	0.2005	2.947 (420)	IL _n →π*/ IL _π →π*
	S ₄	H-2 → L (68) H-1 → L (13) H-4 → L (12)	0.0665	3.299 (376)	IL _n →π*/ IL _π →π*
<i>fac</i> -[ReCl(CO) ₃ (phet)]	S ₁	H → L	0.0006	2.337 (530)	MLCT _{d(Re)→π*} phet
	S ₂	H-2 → L	0.0001	2.409 (514)	IL _n →π*
	S ₃	H-1 → L	0.0280	2.413 (514)	MLCT _{d(Re)→π*} phet LLCT _{n(Cl)→π*} phet
	S ₄	H → L+1	0.0029	2.783 (445)	MLCT _{d(Re)→π*} phet LLCT _{n(Cl)→π*} phet
	S ₅	H-6 → L (20) H-3 → L (80)	0.0001	2.826 (439)	IL _n →π*/ IL _π →π*
	S ₆	H-4 → L (65) H-1 → L+1 (35)	0.457	2.925 (424)	MLCT _{d(Re)→π*} phet

^aH: HOMO; L: LUMO.

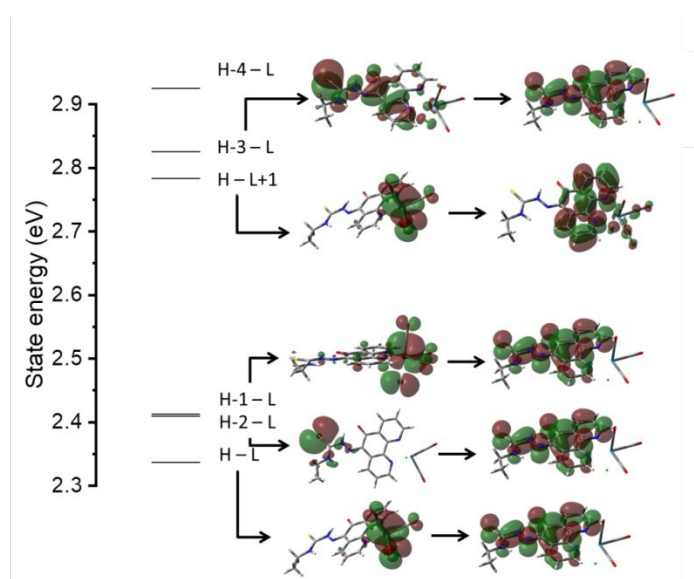


Figure 2. Excited state diagram and the respective frontier orbitals of *fac*-[ReCl(CO)₃(phet)]

The HOMO-LUMO transition in *fac*-[ReCl(CO)₃(phet)] is MLCT in nature although it exhibits low oscillator strength. MLCT transitions with higher molar absorptivities are observed from the HOMO-1 and HOMO-4 molecular orbitals in which the electron density is located at d orbitals of the Re(I) center with some contribution of the unbound electrons in the Cl⁻ ligand. TD-DFT calculations clearly shows the contribution of the internal ligand transition for the lowest lying absorption bands. The S₂ state is IL_{n→π*} in nature and nearly isoenergetic with the MLCT S₃ state. As for the free ligand, the oscillator strength for the IL_{n→π*} is considerably low, however the presence of this state should affect directly the excited state properties of the complex.

Both the free phet ligand and *fac*-[ReCl(CO)₃(phet)] showed weak emission in acetonitrile at room temperature, Figure S9. They displayed a broad emission band in degassed CH₃CN at room temperature with maxima at 525 and 600 nm and luminescence quantum yields (Φ_{em}) of 10⁻⁴ and 10⁻⁵, respectively. The new complex has smaller Stokes shift when compared to the *fac*-[ReCl(CO)₃(phen)], a typical ³MLCT emitter⁵²⁻⁵⁴. Emission quenching was observed in the presence of O₂ (Figure S10), which is an indicative of a spin forbidden radiative decay. Given the low emission quantum yield observed for the complex, it was not possible to measure its emission lifetime in fluid solution at 298 K. Thus time-resolved infrared (TRIR) spectroscopy was employed to unveil the excited state dynamics of the new complex.

TRIR is recognized as powerful technique to investigate the excited state dynamics in metal carbonyl complexes^{55,56}. The CO ligands act as probes of the electron distribution in different excited states, due to the high oscillator strengths of $\nu(\text{CO})$ stretching vibrations and the sensitivity of their energies and bandwidths to changes in the electronic structure. As stated by Schoonover and Strouse⁵⁷, excited-state processes associated with the metal center directly perturb $\nu(\text{CO})$. An MLCT excited state that decreases the electron density at the metal center will shift the $\nu(\text{CO})$ band to higher energy, while a ligand-to-metal charge-transfer state (LMCT) or other transition that increases the metal electron density will shift the $\nu(\text{CO})$ band to lower energy. In the case of intraligand (IL_{n→π*}, IL_{π→π*}) excited states, which neither transfers nor accepts

electron density from the metal center, the population of antibonding orbitals is slightly electron donating relative to the ground state and therefore will cause small shifts in $\nu(\text{CO})$ to lower energy.

In Figure 3, it is shown the transient absorption data at different time-slices following the 450 nm laser excitation. Signals were probed between 2040 and 2005 cm^{-1} in order to monitor changes in the $\nu(\text{C}\equiv\text{O})$ band centered at 2026 cm^{-1} , attributed to CO groups coordinated to the Re(I) center in facial arrangement (Ground state FTIR spectrum is shown Figure S1 of the Supporting Information).

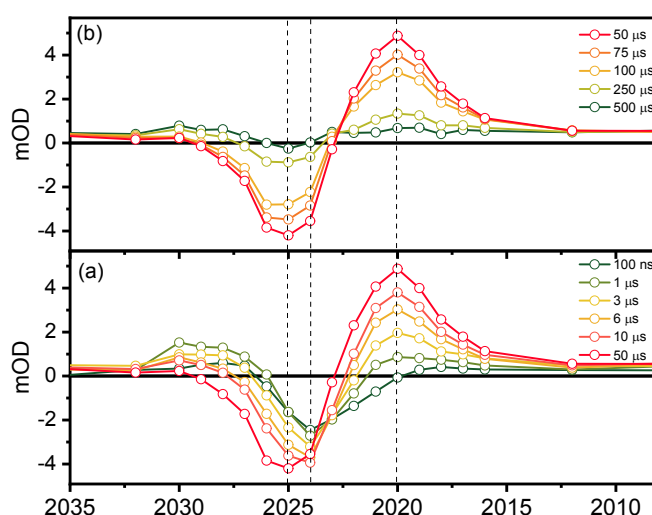
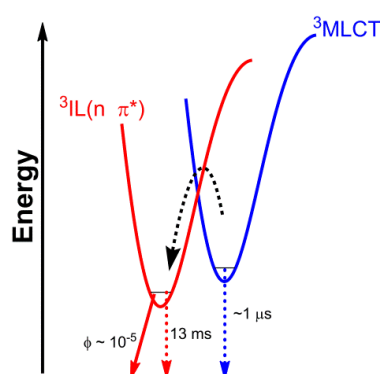


Figure 3. Transient IR spectra (a, b) of *fac*-[ReCl(CO)₃(phet)] in argon degassed acetonitrile at 298 K ($\lambda_{\text{exc}} = 450 \text{ nm}$; 3 mJ per pulse).

The transient spectrum obtained at 100 ns after laser excitation, Figure 3a, is characterized by a bleaching centered at 2024 cm^{-1} , slightly red-shifted in relation to the ground state absorption peak, observed at 2026 cm^{-1} . The bleaching of ground state $\nu(\text{CO})$ absorption band overlaps with a new absorption band at higher energy that reaches its maximum 1 μs after the laser pulse. Concomitantly to this new absorption feature at higher energy, an intense absorption peak appears centered at 2020 cm^{-1} , i.e. lower in energy than the ground state absorption. This peak continues to grow up to 50 μs after the laser pulse, when then slowly decays up to 500 μs after excitation, Figure 3b. Monoexponential fits of the kinetic traces at 2020 cm^{-1} or at 2024 cm^{-1} (Figure S11, Supporting Information) results in very similar lifetimes (11.5 and 13 ms,

respectively). This slow excited state decay is ascribed to the spin-forbidden $^3\text{IL} \rightarrow ^1\text{GS}$ transition.

TRIR data indicate that following excitation, spin-orbit coupling leads to initial population of both a $^3\text{MLCT}$ state, responsible for the high energy transient absorption at $\sim 2029\text{ cm}^{-1}$ and an ^3IL state, responsible for the observed low energy absorption at 2020 cm^{-1} . These states thermally equilibrate within $1\text{ }\mu\text{s}$ after excitation, which results in the interconversion from photons in the $^3\text{MLCT}$ manifold to the lowest lying ^3IL vibronic states. The ligand centered triplet state seems to dominate the excited state decay and is responsible for the low phosphorescence yield observed in fluid solutions at room temperature. The excited state dynamics of *fac*-[ReCl(CO)₃(phet)] in CH₃CN at room temperature is summarized in the Scheme 2.



Scheme 2. Triplet excited state decay dynamics in *fac*-[ReCl(CO)₃(phet)]

3.2. Acid-Basic behavior

Given the changes in the electron density of the coordinated phet ligand under excitation, one can expect changes in the acid-basic behavior from the ground to the excited state. Spectroscopic titrations employing UV-Vis and photoluminescence data could confirm such changes. $10^{-3}\text{ mol L}^{-1}$ CH₃CN solutions of *fac*-[ReCl(CO)₃(phet)] has an apparent pH (pH_{app}) of 6.0. Acidification of the solution with HCl aqueous solutions does not lead to significant spectral changes. On the other hand, addition of NaOH aqueous solutions lead to shifts in the absorption peaks with the formation of four isosbestic points (284, 348, 370 and 455 nm) as well as to the enhancement of the emission intensity, Figure 4. As shown in the inset of Figure 4, the

absorption changes stop after addition of two equivalents of OH^- , which indicates the existence of two acidic sites in the complex.

^1H NMR titrations studies, Figure S12, reveal that the signals at 14.36 and 10.01 ppm, assigned respectively to the H_a and H_b protons (refer to Table 1) are suppressed after addition of OH^- , which is in accordance with the behavior previously observed for similar compounds^{58–61}. Therefore, the acid-basic equilibrium in the *fac*- $[\text{ReCl}(\text{CO})_3(\text{phet})]$ complex can be summarized as show in Scheme 3.

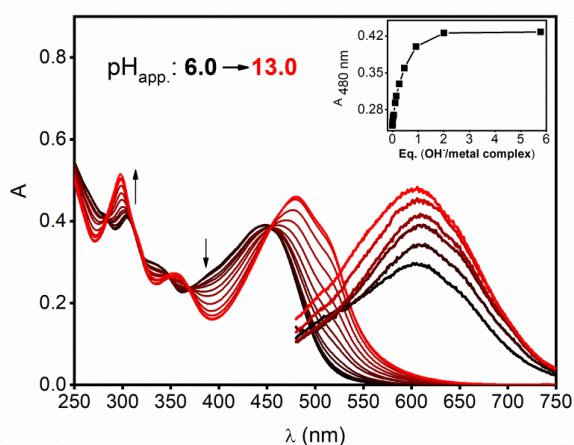
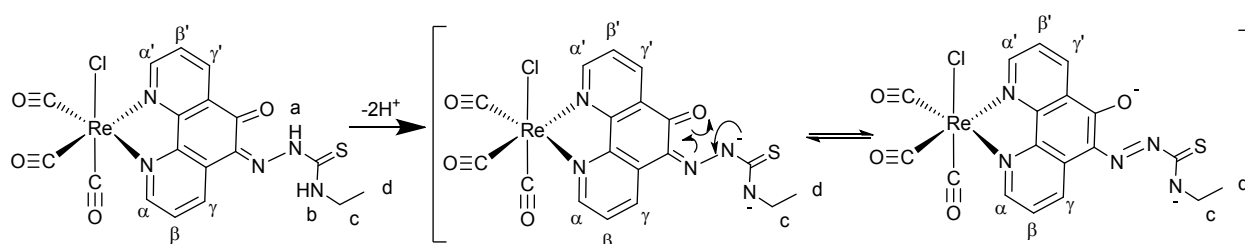


Figure 4. Visible absorption and photoluminescence spectra of *fac*- $[\text{ReCl}(\text{CO})_3(\text{phet})]$ in acetonitrile over the indicated apparent pH range. Inset, the changes at 480 nm with 0→6 molar equivalents of OH^- .



Scheme 3. Acid-basic equilibrium for *fac*- $[\text{ReCl}(\text{CO})_3(\text{phet})]$

Based on the spectroscopic data, the ground-state equilibrium constant pK_β was determined from inflection point observed in the spectrophotometric titration curves, Figure S13, as well as by employing the Equation 1. Despite the existence of two acidic protons, only one inflection point was observed, indicating that the dissociation constants of H_a and H_b are similar to each other. The determined value for $\text{p}\beta$ was 10.0 ± 0.1 . In fact, theoretical calculations reveal that both deprotonation reactions are spontaneous at 298 K, Table S1.

Similar analysis based on pH dependent emission quantum yields according to Equation 2, provided a $\text{pk}\beta^*$ value of 11.4 ± 0.2 for the excited state ⁴⁴, i.e. *fac*-[ReCl(CO)₃(phet)] is a photobase ^{62–66}. Such behavior is in accordance with the excited state dynamics unveiled by TRIR that indicates a triplet ligand centered state as the lowest lying occupied excited state even after MLCT excitation. The electron density enhancement in the π^* orbitals of phet increases its proton affinity.

The sensitivity of the spectral properties of the new *fac*-[ReCl(CO)₃(phet)] complex on proton concentration reveals the ability of this specie to interact with Lewis acids through the thiosemicarbazone moiety, which can be further explored in sensing applications. As a proof of concept, additional titration experiments employing Zn²⁺ ions were carried out also lead to absorption spectral changes, Figure S14. Experimental data indicate a 1:1 molar interaction between the complex and the metal cation (inset Figure S14). Further studies to evaluate the application of the complex as a molecular sensor for metallic cations are in progress. The selectivity could be achieved based on the Pearson acidity of the different cations.

3.3. *Electrochemical Properties*

Cyclic and differential pulse voltammograms of *fac*-[ReCl(CO)₃(phet)] in CH₃CN and propylene carbonate and for the free phet ligand in propylene carbonate are presented in Figure 5.

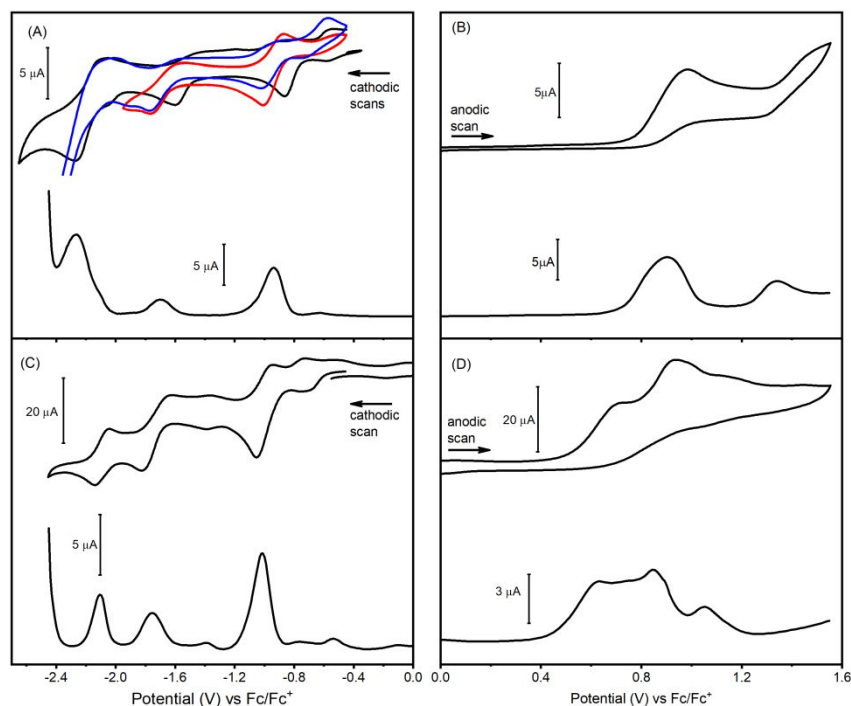


Figure 5. Cyclic and differential pulse voltammograms of argon-aerated solutions of *fac*-[ReCl(CO)₃(phet)] in acetonitrile (—) or propylene carbonate in different scan ranges (—, —) (A, B). In (C,D) data for the free phet ligand in propylene carbonate is shown. The concentration of both species is 4×10^{-3} mol L⁻¹; scan rate = 100mV/s with 0.1 M TBAPF₆ as supporting electrolyte.

The anodic scan of *fac*-[ReCl(CO)₃(phet)] solutions reveal two peaks at 0.94 and 1.34 V, Figure 5B, attributed respectively to the irreversible one electron oxidation of the coordinated phet and the metal centers. Such attributions are based on the comparison with voltammetric data obtained for the free ligand, Figure 5C, and those for the parental complex *fac*-[ReCl(CO)₃(phdo)], Figure S15. The free phet ligand exhibits at least three irreversible oxidation peaks between 0.4 and 1.2 V, similar to other aromatic thiosemicarbazone derivatives^{67,68} and that are partially inhibited after coordination. In *fac*-[ReCl(CO)₃(phet)], the first oxidation process occurs in the thiosemicarbazone moiety, particularly in the non-bonding orbitals of the sulfur atom, as evidenced by TD-DFT calculations of the *fac*-[ReCl(CO)₃(phet)]^{•+} radical (Figure S16). The most stable SOMO in the 1 e⁻ oxidized *fac*-[ReCl(CO)₃(phet)] are centered at the non-bonding p orbitals of S atom in the thiosemicarbazone group.

At cathodic scans, both free phet and *fac*-[ReCl(CO)₃(phet)] exhibit multiple reduction processes in the investigated electrochemical window. The free ligand exhibits a first one electron reduction wave at $E_{1/2} = -1.05$ V. The attribution of the number of electrons involved in the (quasi)reversible waves was determined based on the comparison with the experimental ΔE values obtained for the standard ferrocene/ferrocenium redox couple (Figure S17a). Reversibility studies (Figures S17b) of this reduction process indicate the occurrence of a coupled chemical reaction following the electrochemical step, as the anodic peak current is not linear to the square root of the scan rate. The following cathodic peaks at -1.75 and -2.05 V correspond to one electron reduction processes which show the same dependence on the scan rate as observed for the first sweep.

For the *fac*-[ReCl(CO)₃(phet)] complex in acetonitrile, a first one electron reduction wave at -0.86 V is observed. Different from the free ligand, the first reduction of the complex does not trigger a chemical reaction in the investigated scan rate interval (Figure S17c, d). A second process is observed at -1.70 V which exhibits similar behavior of the free ligand. At more cathodic potentials, it can be observed two sequential one electron reduction processes at very close potentials that lead to chemical changes at the electroactive specie, as the anodic processes correspondent to the first reduction processes cannot be observed after scan up to -2.40 V, Figure 5A.

DFT calculations, Figure 6, reveal that the three first reduction processes are ligand based, although it can be observed an electron delocalization on the [Re(CO)₃] moiety in the most stable SOMO of the one electron-reduced radical specie. The bi-anion potentially formed after four electron reduction exhibits an HOMO in which electron density is spread all over the phet π^* orbitals and rhenium d orbitals. As a result, Re-Cl bond distance increases to 5.006 Å (twice the value observed for the neutral complex). Thus, multiple reduction of *fac*-[ReCl(CO)₃(phet)] results in the labilization of the Cl⁻ ligand and formation of a solvato complex in CH₃CN. In propylene carbonate, a catalytic process is clearly triggered after -2.05 V, which led us to evaluate the potential application of *fac*-[ReCl(CO)₃(phet)] as electrocatalyst for CO₂ reduction, an important reaction for green chemistry.

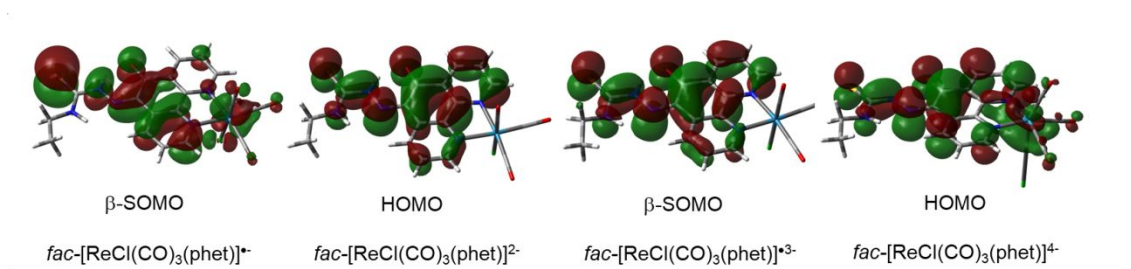


Figure 6. Lowest lying full (HOMO) or singly (SOMO) occupied molecular orbitals in *fac*-[ReCl(CO)₃(phet)] after consecutive one electron reduction.

Cyclic voltammograms of *fac*-[ReCl(CO)₃(phet)] in Ar and CO₂-saturated acetonitrile are shown in Figure 7. In the presence of CO₂, it can be observed a catalytic process with onset potential at -1.92 V. When compared to the Lhen's catalyst *fac*-[ReCl(CO)₃(bpy)]⁺, bpy = 2,2'-bipyridine, the onset potential is 270 mV more negative. As observed for other Re(I) polypyridine complexes, addition of protic solvents (H₂O) led to a decrease (up to 0.4 V) in the onset potential, Figure 10 inset. As water is added to medium, one can observe that the first reduction peak, initially at -0.86 V in net acetonitrile, is shifted to more negative potentials (-0.98 V). This behavior probably occurs with the second redox peak that is overlapped by the catalytic wave. The decrease on the onset potential suggests that the CO₂ reduction by *fac*-[ReCl(CO)₃(phet)] should follow a similar mechanism than that proposed for other Re(I) complexes^{27,56,69}. GC measurements have confirmed that CO is the main reduction product. CO is only detected in CO₂-saturated solutions containing the Re(I) complex as evidenced by control experiments in the absence of either the electrocatalyst or the substrate.

The turnover number (TOF) for the electrocatalyst can be calculated by applying the equation 3⁷⁰, where i_{cat} and i_{p} are respectively the catalytic and peak currents in the presence and absence of CO₂, $n_{\text{cat}}=2$ is the number of electrons involved in the catalytic, F is the Faraday constant, $x=1$ is the kinetic order of the reaction involving the substrate⁷¹, k is the second order rate constant for the reaction and v is the scan rate. The CO₂ concentration in the acetonitrile solution was assumed to be 0.28 mol L⁻¹⁷². Values of TOF and k are listed at Table 4 along with other reported Re-based CO₂ reduction electrocatalysts. One can observe that the determined TOF for *fac*-[ReCl(CO)₃(phet)] lies on the same range than other Re(I) complexes with

polypyridine ligands with extended π conjugation, but below the best Re(I)-catalyst, *fac*-[ReCl(CO)₃(bipy-tBu)], bipy-tBu = 4,4'-di-tert-butyl-2,2'-dipyridyl, reported so far²⁷.

$$TOF = k[CO_2]^X = \frac{Fv}{RT} \left(\frac{0.4463}{n_{cat}} \right)^2 \left(\frac{i_{cat}}{i_p} \right)^2 \quad (3)$$

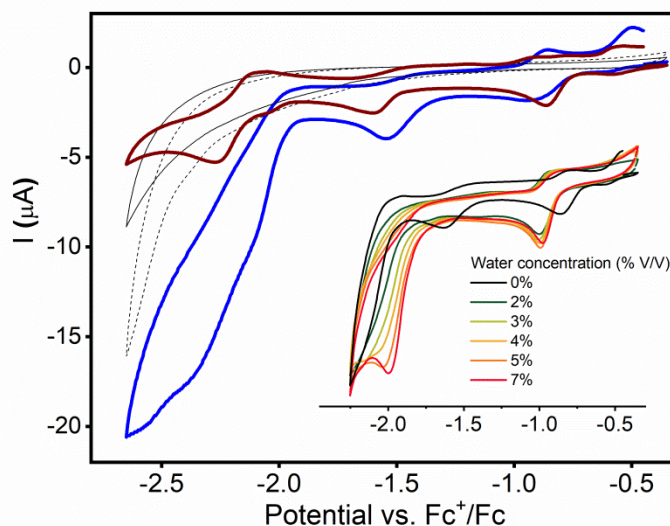
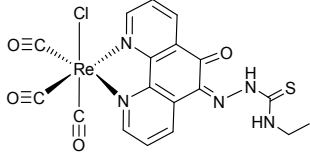
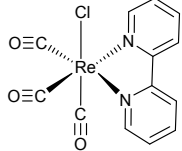
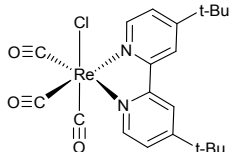
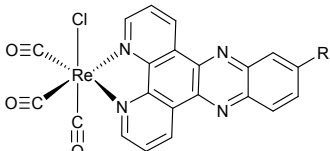
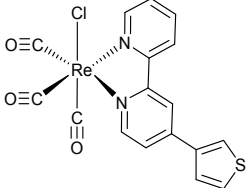
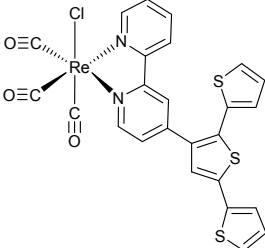
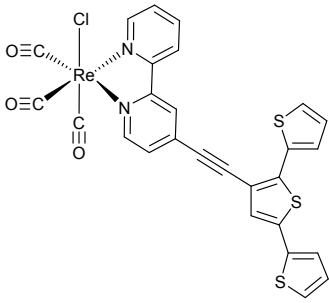
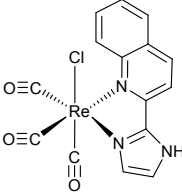


Figure 7. CVs of *fac*-[ReCl(CO)₃(phet)] in anhydrous acetonitrile saturated with Ar (—) or in CO₂ (—) or in CO₂ (----) saturated solutions at the absence of the Re(I) complex. *Inset:* CVs of *fac*-[ReCl(CO)₃(phet)] in CO₂ saturated solutions with different water amounts. Scan rate of 0.1 V.s⁻¹; 0.1 M TBAPF₆ as supporting electrolyte.

Table 4. second order rate constant at 298 K and TOF values for CO₂ reduction employing different Re(I)-based electrocatalysts.

Complex	k (mol ⁻¹ L s ⁻¹)	TOF (s ⁻¹)	Ref
	10	2.8	this work
	100 ⁷³ , 60 ⁷⁴	26 ⁷³ , 12 ⁷⁵	74-76
	1000	>200	27
 <div style="display: inline-block; vertical-align: middle; margin-left: 10px;"> <p>R = CF₃</p> <p>R = NO₂</p> <p>R = H</p> <p>R = ^tBu</p> </div>	--	1.5 0.3 0.3 0.4	76
	50	14	77
	28	8	77
	84	24	77
	5	1.4	78

Controlled potential electrolysis (CPE) in a gas tight H-cell, followed by GC analysis of the headspace was carried out, Figure 8, allowing to obtain the faradaic efficiency (η_F) for CO production and the respective turnover number (TON). For *fac*-[ReCl(CO)₃(phet)], a η_F of $84\pm 5\%$ and a TON of 24 ± 1 were determined at an applied potential of -2.25 V. For reference, Lhen's catalyst, *fac*-[ReCl(CO)₃(bpy)], in the same experimental setup exhibited $\eta_F = 92\pm 5\%$ and TON = 20 ± 1 at an applied potential of -1.85 V.

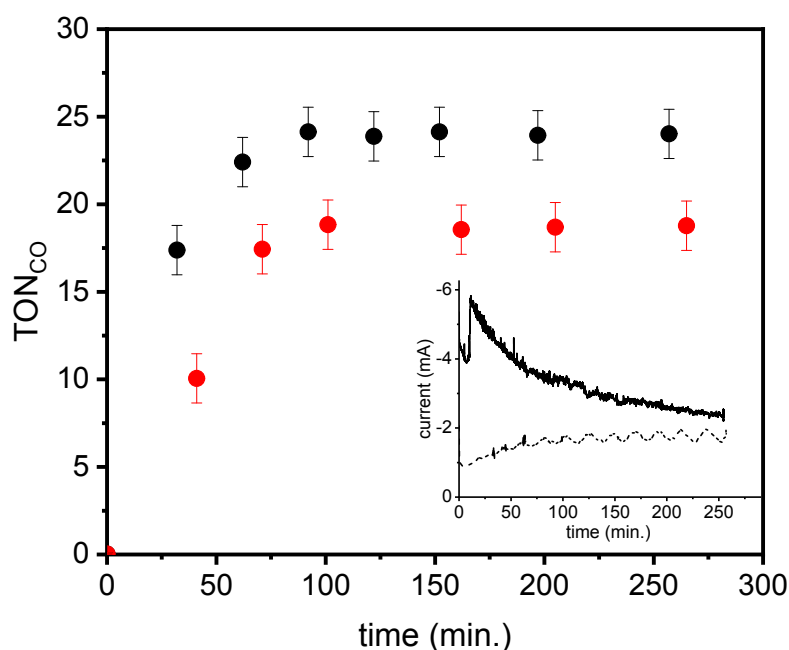


Figure 8. Turnover number obtained for CO production from CO₂ saturated anhydrous CH₃CN solution in the presence of *fac*-[ReCl(CO)₃(phet)] under -2.25 V vs Fc⁺/Fc (•) or *fac*-[ReCl(CO)₃(bpy)] under -1.95 V vs Fc⁺/Fc (•). *Inset:* Current vs. time profile for the electrolysis with *fac*-[ReCl(CO)₃(phet)] in CO₂ (—) or Ar (---) saturated solutions.

The higher onset potential for CO₂ reduction by *fac*-[ReCl(CO)₃(phet)] in relation to that observed for *fac*-[ReCl(CO)₃(bpy)] is in agreement with DFT calculations which show that Cl⁻ release occurs only after four electrons are transferred to the *fac*-[ReCl(CO)₃(phet)] complex. The formation of a 5 five coordinated [Re(NN)(CO)₃] specie has been identified as a required step for CO₂ reduction^{27,79}. As only the 2e⁻ reduction product (CO) was identified, the additional electrons in centered at π^* orbitals of the coordinated phet ligand seems to not take part in the catalytic reaction, which also explains the relatively

low faradaic efficiency and the modest TON in relation to the state of art electrocatalysts. Such observations can drive future structural modifications in the phet ligand toward improving the catalytic performance. Additionally, the presence of the thiosemicarbazone moiety also allows the hybridization of the electrocatalyst in suitable substrates, which is recognized as an efficient strategy^{80,81} to enhance the stability and performance of Re(I)-based CO₂ catalyst.

4. Conclusions

The new complex, *fac*-[ReCl(CO)₃(phet)], combines interesting properties of typical Re(I) polypyridine complexes such as *fac*-[ReCl(CO)₃(phen)] or *fac*-[ReCl(CO)₃(bpy)] with those observed for species containing thiosemicarbazone groups. The low energy absorption bands lies on the visible region of the spectrum and exhibit high molar absorptivities ($\sim 10^4$ L mol⁻¹ cm⁻¹) as a result of an overlap between MLCT_{Re→phet} and IL_{phet(n→π*)} transitions. The low lying ligand centered excited state plays a major role on the excited state dynamics as evidenced by TRIR measurements. In fluid solutions at room temperature, the typical MLCT emission observed for other Re(I) complexes is greatly inhibited and only ligand centered phosphorescence is observed with low quantum yields. The population of the ³IL_{phet(n→π*)} excited state also leads to changes in the acid-basic behavior in relation to the ground state as a result of variations in the charge density in the N atoms of the thiosemicarbazone group. The coordination of phet to the Re(I) cation also leads to the observation of multiple quasi-reversible reduction processes. Three consecutive one electron reduction of the coordinated ligand is observed and after the fourth reduction, Cl⁻ release occurs. The complex is able to act as an electrocatalysis for CO₂ reduction into CO with performance comparable to that observed for Lhen's catalyst, *fac*-[ReCl(CO)₃(bpy)]. The fundamental characterization studies carried out here opens new perspectives for future applications of Re(I) complexes containing thiosemicarbazone groups.

5. Conflicts of interest

There are no conflicts to declare

6. Acknowledgements

This work was supported by Fundação de Amparo à Pesquisa do Estado de Minas Gerais (FAPEMIG, PPM-00220-17 and APQ-03017-16), Conselho Nacional de Desenvolvimento Científico e Tecnológico (CNPq, 406392/2018-8, 310303/2018-4, 305432/2017-6 and 307443/2015-9) and Coordenação de Aperfeiçoamento de Pessoal de Nível Superior (CAPES). The authors are also thankful to the Grupo de Materiais Inorgânicos do Triângulo (GMIT), a research group supported by FAPEMIG (APQ-00330-14). A.O.T.P. is thankful to Alexander Von Humboldt Foundation for the financial support. The work at Brookhaven National Laboratory (R. N. S.) was carried out under contract DE-SC0012704 with the U.S. Department of Energy, Office of Science, Office of Basic Energy Sciences.

7. References

- 1 M. Wrighton and D. L. Morse, *J. Am. Chem. Soc.*, 1974, **96**, 998–1003.
- 2 S. M. Fredericks, J. C. Luong and M. S. Wrighton, *J. Am. Chem. Soc.*, 1979, **101**, 7415–7417.
- 3 P. J. Giordano and M. S. Wrighton, *J. Am. Chem. Soc.*, 1979, **101**, 2888–2897.
- 4 M. S. Wrighton, D. L. Morse and L. Pdungsap, *J. Am. Chem. Soc.*, 1975, **97**, 2073–2079.
- 5 A. W.-T. Choi, V. M.-W. Yim, H.-W. Liu and K. K.-W. Lo, *Chem. - A Eur. J.*, 2014, **20**, 9633–9642.
- 6 C. Wang, *J. Lumin.*, 2014, **145**, 531–538.
- 7 L. D. Ramos, R. N. Sampaio, F. F. De Assis, K. T. De Oliveira, P. Homem-De-Mello, A. O. T. Patrocínio and K. P. M. Frin, *Dalt. Trans.*, 2016, **45**, 11688–11698.
- 8 T. Yu, D. P.-K. Tsang, V. K.-M. Au, W. H. Lam, M.-Y. Chan and V. W.-W. Yam, *Chem. - A Eur. J.*, 2013, **19**, 13418–13427.
- 9 M. Mauro, E. Q. Procopio, Y. Sun, C.-H. Chien, D. Donghi, M. Panigati, P. Mercandelli, P. Mussini, G. D'Alfonso and L. De Cola, *Adv. Funct. Mater.*, 2009, **19**, 2607–2614.
- 10 N. J. Lundin, A. G. Blackman, K. C. Gordon and D. L. Officer, *Angew. Chemie Int. Ed.*, 2006, **45**, 2582–2584.
- 11 S. K. Mizoguchi, A. O. T. Patrocínio and N. Y. Murakami Iha, *Synth. Met.*, 2009, **159**, 2315–2317.
- 12 L. A. Faustino, A. E. Hora Machado and A. O. T. Patrocínio, *Inorg. Chem.*, 2018, **57**, 2933–2941.
- 13 A. S. Polo, M. K. Itokazu, K. M. Frin, A. O. de Toledo Patrocínio and N. Y. Murakami Iha, *Coord. Chem. Rev.*, 2006, **250**, 1669–1680.
- 14 A. O. T. Patrocínio, K. P. M. Frin and N. Y. Murakami Iha, *Inorg. Chem.*, 2013, **52**, 5889–5896.
- 15 N. Hoffmann, *ChemSusChem*, 2012, **5**, 352–371.

- 16 X. Yi, J. Zhao, W. Wu, D. Huang, S. Ji and J. Sun, *Dalt. Trans.*, 2012, **41**, 8931.
- 17 K. K.-W. Lo, *Acc. Chem. Res.*, 2015, **48**, 2985–2995.
- 18 S. F. Sousa, B. L. Souza, C. L. Barros and A. O. T. Patrocínio, *Int. J. Photoenergy*, 2019, **2019**, 1–23.
- 19 J. Hawecker, J.-M. Lehn and R. Ziessel, *J. Chem. Soc., Chem. Commun.*, 1984, 328–330.
- 20 T. Morimoto, T. Nakajima, S. Sawa, R. Nakanishi, D. Imori and O. Ishitani, *J. Am. Chem. Soc.*, 2013, **135**, 16825–16828.
- 21 J. Agarwal, E. Fujita, H. F. Schaefer and J. T. Muckerman, *J. Am. Chem. Soc.*, 2012, **134**, 5180–5186.
- 22 E. Portenkirchner, E. Kianfar, N. S. Sariciftci and G. Knör, *ChemSusChem*, 2014, **7**, 1347–1351.
- 23 N. Elgrishi, M. B. Chambers, X. Wang and M. Fontecave, *Chem. Soc. Rev.*, 2017, **46**, 761–796.
- 24 L. Rotundo, E. Azzi, A. Deagostino, C. Garino, L. Nencini, E. Priola, P. Quagliotto, R. Rocca, R. Gobetto and C. Nervi, *Front. Chem.*, 2019, **7**, 417.
- 25 Y. Kuramochi, O. Ishitani and H. Ishida, *Coord. Chem. Rev.*, 2018, **373**, 333–356.
- 26 A. Nakada and O. Ishitani, *ACS Catal.*, 2018, **8**, 354–363.
- 27 J. M. Smieja and C. P. Kubiak, *Inorg. Chem.*, 2010, **49**, 9283–9289.
- 28 J. J. Teesdale, A. J. Pistner, G. P. A. Yap, Y.-Z. Ma, D. A. Lutterman and J. Rosenthal, *Catal. Today*, 2014, **225**, 149–157.
- 29 F. R. Pavan, P. I. d. S. Maia, S. R. A. Leite, V. M. Deflon, A. A. Batista, D. N. Sato, S. G. Franzblau and C. Q. F. Leite, *Eur. J. Med. Chem.*, 2010, **45**, 1898–1905.
- 30 R. Carballo, J. S. Casas, E. García-Martínez, G. Pereiras-Gabián, A. Sánchez, J. Sordo, E. M. Vázquez-López, J. C. Garcia-Monteagudo and U. Abram, *J. Organomet. Chem.*, 2002, **656**, 1–10.
- 31 R. Carballo, J. S. Casas, E. García-Martínez, G. Pereiras-Gabián, A. Sánchez, J. Sordo and E. M. Vázquez-López, *Inorg. Chem.*, 2003, **42**, 6395–6403.
- 32 I. G. Santos, U. Abram, R. Alberto, E. V. Lopez and A. Sanchez, *Inorg. Chem.*, 2004, **43**, 1834–1836.
- 33 A. Núñez-Montenegro, R. Carballo and E. M. Vázquez-López, *J. Inorg. Biochem.*, 2014, **140**, 53–63.
- 34 M. Bakir and O. Brown, *J. Mol. Struct.*, 2013, **1032**, 118–125.
- 35 M. Bakir and O. Brown, *J. Mol. Struct.*, 2009, **930**, 65–71.
- 36 J. Dickeson and L. Summers, *Aust. J. Chem.*, 1970, **23**, 1023.
- 37 Y. Jiang and C.-F. Chen, *Synlett*, 2010, **2010**, 1679–1681.
- 38 R. H. Zheng, H. C. Guo, H. J. Jiang, K. H. Xu, B. B. Liu, W. L. Sun and Z. Q. Shen, *Chinese Chem. Lett.*, 2010, **21**, 1270–1272.
- 39 M. Kaplanis, G. Stamatakis, V. D. Papakonstantinou, M. Paravatou-Petsotas, C. A. Demopoulos and C. A. Mitsopoulou, *J. Inorg. Biochem.*, 2014, **135**, 1–9.
- 40 F. Prado, S. Sousa, A. E. Machado and A. O. Patrocínio, *J. Braz. Chem. Soc.*, 2016, **28**, 1741–1751.
- 41 S. F. Sousa, R. N. Sampaio, N. M. Barbosa Neto, A. E. H. Machado and A. O. T. Patrocínio, *Photochem. Photobiol. Sci.*, 2014, **13**, 1213–1224.
- 42 A. Juris, V. Balzani, F. Barigelletti, S. Campagna, P. Belser and A. Von Zelewsky,

- ChemInform*, 1988, **19**, 85–277.
- 43 R. N. Sampaio, D. C. Grills, D. E. Polyansky, D. J. Szalda and E. Fujita, *J. Am. Chem. Soc.*, 2020, **142**, 2413–2428.
- 44 A. P. de Silva, H. Q. N. Gunaratne, P. L. M. Lynch, A. J. Patty and G. L. Spence, *J. Chem. Soc. Perkin Trans. 2*, 1993, 1611.
- 45 B. A. F. Previdello, F. R. de Carvalho, A. L. Tessaro, V. R. de Souza and N. Hioka, *Quim. Nova*, 2006, **29**, 600–606.
- 46 K. N. Farrugia, D. Makuc, A. Podborska, K. Szaciłowski, J. Plavec and D. C. Magri, *Org. Biomol. Chem.*, 2015, **13**, 1662–1672.
- 47 J. Tomasi, B. Mennucci and R. Cammi, *Chem. Rev.*, 2005, **105**, 2999–3094.
- 48 H. B. Shawish, M. Paydar, C. Y. Looi, Y. L. Wong, E. Movahed, S. N. A. Halim, W. F. Wong, M.-R. Mustafa and M. J. Maah, *Transit. Met. Chem.*, 2014, **39**, 81–94.
- 49 T. K. Venkatachalam, G. K. Pierens and D. C. Reutens, *Magn. Reson. Chem.*, 2014, **52**, 98–105.
- 50 D. . Striplin and G. . Crosby, *Coord. Chem. Rev.*, 2001, **211**, 163–175.
- 51 K. P. M. Frin and V. M. Nascimento, *J. Braz. Chem. Soc.*, 2015, **27**, 179–185.
- 52 A. J. Lees, *Chem. Rev.*, 1987, **87**, 711–743.
- 53 L. A. Worl, R. Duesing, P. Chen, L. Della Ciana and T. J. Meyer, *J. Chem. Soc. Dalton Trans.*, 1991, 849.
- 54 A. O. T. Patrocínio, M. K. Brennaman, T. J. Meyer and N. Y. Murakami Iha, *J. Phys. Chem. A*, 2010, **114**, 12129–12137.
- 55 J. M. Butler, M. W. George, J. R. Schoonover, D. M. Dattelbaum and T. J. Meyer, *Coord. Chem. Rev.*, 2007, **251**, 492–514.
- 56 J. Dyer, W. J. Blau, C. G. Coates, C. M. Creely, J. D. Gavey, M. W. George, D. C. Grills, S. Hudson, J. M. Kelly, P. Matousek, J. J. McGarvey, J. McMaster, A. W. Parker, M. Towrie and J. A. Weinstein, *Photochem. Photobiol. Sci.*, 2003, **2**, 542.
- 57 J. R. Schoonover and G. F. Strouse, *Chem. Rev.*, 1998, **98**, 1335–1356.
- 58 L. S. Evans, P. A. Gale, M. E. Light and R. Quesada, *Chem. Commun.*, 2006, 965.
- 59 T. Gunnlaugsson, M. Glynn, G. M. Tocci (née Hussey), P. E. Kruger and F. M. Pfeffer, *Coord. Chem. Rev.*, 2006, **250**, 3094–3117.
- 60 R. M. Duke, E. B. Veale, F. M. Pfeffer, P. E. Kruger and T. Gunnlaugsson, *Chem. Soc. Rev.*, 2010, **39**, 3936.
- 61 K. Pandurangan, J. A. Kitchen and T. Gunnlaugsson, *Tetrahedron Lett.*, 2013, **54**, 2770–2775.
- 62 A. R. Watkins, *J. Chem. Soc. Faraday Trans. 1 Phys. Chem. Condens. Phases*, 1972, **68**, 28.
- 63 P. J. Kovi and S. G. Schulman, *Anal. Chem.*, 1973, **45**, 989–991.
- 64 C. J. Marzocco, G. Deckey and A. M. Halpern, *J. Phys. Chem.*, 1982, **86**, 4937–4941.
- 65 S. J. Formosinho and L. G. Arnaut, *J. Photochem. Photobiol. A Chem.*, 1993, **75**, 21–48.
- 66 R. M. O'Donnell, R. N. Sampaio, G. Li, P. G. Johansson, C. L. Ward and G. J. Meyer, *J. Am. Chem. Soc.*, 2016, **138**, 3891–3903.
- 67 G.-O. Buica, L. Birzan, V. Tecuceanu, A. C. Razus, G.-L. Arnold and E.-M. Ungureanu, *Electroanalysis*, 2017, **29**, 93–102.
- 68 S. A. M. Refaey, A. A. Hassan and H. S. Shehata, *Int. J. Electrochem. Sci.*, 2008, **3**, 325–337.

- 69 G. F. Manbeck, J. T. Muckerman, D. J. Szalda, Y. Himeda and E. Fujita, *J. Phys. Chem. B*, 2015, **119**, 7457–7466.
- 70 J. M. Smieja, E. E. Benson, B. Kumar, K. A. Grice, C. S. Seu, A. J. M. Miller, J. M. Mayer and C. P. Kubiak, *Proc. Natl. Acad. Sci.*, 2012, **109**, 15646–15650.
- 71 T. R. O'Toole, B. P. Sullivan, M. R.-M. Bruce, L. D. Margerum, R. W. Murray and T. J. Meyer, *J. Electroanal. Chem. Interfacial Electrochem.*, 1989, **259**, 217–239.
- 72 A. Gennaro, A. A. Isse and E. Vianello, *J. Electroanal. Chem. Interfacial Electrochem.*, 1990, **289**, 203–215.
- 73 D. C. Grills, Y. Matsubara, Y. Kuwahara, S. R. Golisz, D. A. Kurtz and B. A. Mello, *J. Phys. Chem. Lett.*, 2014, **5**, 2033–2038.
- 74 E. Portenkirchner, K. Oppelt, C. Ulbricht, D. A. M. Egbe, H. Neugebauer, G. Knör and N. S. Sariciftci, *J. Organomet. Chem.*, 2012, **716**, 19–25.
- 75 F. Franco, C. Cometto, C. Garino, C. Minero, F. Sordello, C. Nervi and R. Gobetto, *Eur. J. Inorg. Chem.*, 2015, **2015**, 296–304.
- 76 Y. Liang, M. T. Nguyen, B. J. Holliday and R. A. Jones, *Inorg. Chem. Commun.*, 2017, **84**, 113–117.
- 77 C. Sun, S. Prosperini, P. Quagliotto, G. Viscardi, S. S. Yoon, R. Gobetto and C. Nervi, *Dalt. Trans.*, 2016, **45**, 14678–14688.
- 78 S. Sinha, E. K. Berdichevsky and J. J. Warren, *Inorganica Chim. Acta*, 2017, **460**, 63–68.
- 79 M. L. Clark, P. L. Cheung, M. Lessio, E. A. Carter and C. P. Kubiak, *ACS Catal.*, 2018, **8**, 2021–2029.
- 80 A. Ge, B. Rudshiteyn, P. E. Videla, C. J. Miller, C. P. Kubiak, V. S. Batista and T. Lian, *Acc. Chem. Res.*, 2019, **52**, 1289–1300.
- 81 L. A. Faustino, B. L. Souza, B. N. Nunes, A.-T. Duong, F. Sieland, D. W. Bahnemann and A. O. T. Patrocínio, *ACS Sustain. Chem. Eng.*, 2018, **6**, 6073–6083.

Spectroscopic characterization of a new Re(I) tricarbonyl complex with a thiosemicarbazone derivative: towards sensing and electrocatalytic applications

Table of contents entry

A novel Re(I) complex with a thiosemicarbazone derivative is described and fully characterized. Its was further explored as CO₂ reduction electrocatalyst, being the first complex with a thiosemicarbazone derivative applied to this goal.

